Available online at www.sciencedirect.com
ScienceDirect
Journal of Solid State Chemistry 180 (2007) 1421–1430
JOURNAL OF SOLID STATE CHEMISTRY
www.elsevier.com/locate/jssc

Host-sensitized luminescence of Dy^{3+}, Pr^{3+}, Tb^{3+} in polycrystalline $CaIn_2O_4$ for field emission displays

Xiaoming Liu[a,b], Ran Pang[a,b], Qin Li[a,b], Jun Lin[a,*]

[a]*Key Laboratory of Rare Earth Chemistry and Physics, Changchun Institute of Applied Chemistry, Chinese Academy of Sciences, Changchun 130022, PR China*
[b]*Graduate University of the Chinese Academy of Sciences, Beijing 100049, PR China*

Received 7 October 2006; received in revised form 11 December 2006; accepted 23 January 2007
Available online 20 February 2007

Abstract

$CaIn_2O_4:Dy^{3+}/Pr^{3+}/Tb^{3+}$ blue–white/green/green phosphors were prepared by the Pechini sol–gel process. X-ray diffraction (XRD), field emission scanning electron microscopy (FE-SEM), diffuse reflectance, photoluminescence (PL) and cathodoluminescence (CL) spectra as well as lifetimes were utilized to characterize the samples. The XRD results reveal that the samples begin to crystallize at 800 °C and pure $CaIn_2O_4$ phase can be obtained after annealing at 900 °C. The FE-SEM images indicate that the $CaIn_2O_4:Dy^{3+}$, $CaIn_2O_4:Pr^{3+}$ and $CaIn_2O_4:Tb^{3+}$ samples consist of spherical grains with size around 200–400 nm. Under the excitation of ultraviolet light and low-voltage electron beams (1–5 kV), the $CaIn_2O_4:Dy^{3+}$, $CaIn_2O_4:Pr^{3+}$ and $CaIn_2O_4:Tb^{3+}$ phosphors show the characteristic emissions of Dy^{3+} ($^4F_{9/2}$–$^6H_{15/2}$ and $^4F_{9/2}$–$^6H_{13/2}$ transitions, blue–white), Pr^{3+} ($^3P_0$–$^3H_4$, $^1D_2$–$^3H_4$ and $^3P_1$–$^3H_5$ transitions, green) and Tb^{3+} ($^5D_4$–$^7F_{6,5,4,3}$ transitions, green), respectively. All the luminescence is resulted from an efficient energy transfer from the $CaIn_2O_4$ host lattice to the doped Dy^{3+}, Pr^{3+} and Tb^{3+} ions, and the corresponding luminescence mechanisms have been proposed.

Keywords: $CaIn_2O_4$; Terbium; Praseodymium; Dysprosium; Luminescence

1. Introduction

Field emission displays (FEDs) offer the potential of achieving comparable or superior levels of performance to cathode ray tubes (CRTs). However, FEDs must be operated at significantly lower excitation voltages ($\leqslant$5 kV) and higher current densities (10–100 μA/cm^2) than CRTs. Thus, the phosphors for FEDs are required to have a higher efficiency at low voltages, higher resistance to current saturation, longer service time and equal or better chromaticity than CRT phosphors [1–6]. While many efficient sulfide-based compounds have been explored as possible low-voltage phosphors, the volatility of sulfur has prohibited their use in the FEDs. Sulfide-base phosphors often degrade under the high-energy electron bombardment due to dissociation of the cation-sulfur bonds. The process generates corrosive sulfur-bearing gas species that contaminate emission tips and shorten the device lifetime. Oxide phosphors are chemically stable, yet most of phosphors are insulators. When they are excited by low-voltage electrons with high-density, charging problems often occur. Therefore, in order to improve the performance of FED devices, it is necessary to find novel phosphors with high luminescence efficiency, good stability and reasonable conductivity [7–12].

The lanthanide (Ln) ions have been playing an important role in modern lighting and display fields due to the abundant emission colors based on their 4*f*–4*f* (for trivalent Ln^{3+} except Ce^{3+}) or 5*d*–4*f* transitions (for divalent Ln^{2+}) [13]. However, the *f*–*f* transitions of Ln^{3+} ions have low oscillator strength (10^{-6}) due to their forbidden features by the parity selection rule, resulting in the low excitation efficiency. As a result, the sensitization of Ln^{3+} ions by other species with allowed broad excitation bands seems very important in enhancing the excitation and emission

*Corresponding author. Key Laboratory of Rare Earth Chemistry and Physics, Changchun Institute of Applied Chemistry, Chinese Academy of Sciences, Changchun 130022, PR China. Fax: +86 431 85698041.
E-mail address: jlin@ciac.jl.cn (J. Lin).

0022-4596/$ - see front matter © 2007 Elsevier Inc. All rights reserved.
doi:10.1016/j.jssc.2007.01.034

efficiencies of Ln^{3+} ions. Host sensitization for Ln^{3+} ions, i.e., efficient energy transfer from the host to Ln^{3+} ions, is one of the most significant routes to realize the efficient emission of Ln^{3+} ions, such as YVO_4:Eu^{3+} [14]. The luminescence of trivalent dysprosium Dy^{3+} mainly consists of narrow lines in the blue (470–500 nm, $^4F_{9/2}$–$^6H_{15/2}$) and yellow (570–600 nm, $^4F_{9/2}$–$^6H_{13/2}$) wavelength region. At a suitable yellow-to-blue intensity ratio, Dy^{3+} will emit white light. However, unlike the most frequently used Eu^{3+} and Tb^{3+} (in oxide hosts), which have allowed charge-transfer absorption band (CTB) or $4f^8$–$4f^7 5d$ absorption band in the UV region, respectively, the excitation spectrum of Dy^{3+} consists of only narrow *f–f* transition lines from 300 to 500 nm (both CTB and $4f^9$–$4f^8 5d$ band of Dy^{3+} are located below 200 nm) [15]. As a result, the luminescence of Dy^{3+} cannot be excited with 254 nm UV light efficiently, and the excitation can occur only through the *f–f* transitions with low oscillator strength (10^{-6}) due to their forbidden features by the parity selection rule [13]. This drawback of Dy^{3+} luminescence can be overcome by sensitization, such as host sensitization in YVO_4:Dy^{3+} and ion sensitization in $Ca_2Gd_8(SiO_4)_6O_2$:Pb^{2+}, Dy^{3+} [16,17]. Trivalent praseodymium (Pr^{3+}) mainly emits efficiently between the blue and the red region, depending on the host materials, the concentration and the excitation conditions. The Tb^{3+} is also a well-known green emitting ion due to its $^5D_4$–$^7F_5$ (543 nm) transition [13]. All these ions need sensitizing to realize their efficient emissions.

Oxide semiconductors have good stability and reasonable conductivity. If host sensitizing effect occurs in Ln^{3+}-doped oxide semiconductors, efficient phosphor materials for photoluminescence (PL) and FEDs might be obtained. $CaIn_2O_4$ is a semiconductor with a reported bandgap (E_g) of 3.9 eV, belonging to the ordered $CaFe_2O_4$ structures with the $Pca2_1$ or $Pbcm$ space group and the lattice parameters $a = 9.70$, $b = 11.30$ and $c = 3.21$ Å for $Z = 4$ [18]. $CaIn_2O_4$ shows only weak self-activated blue luminescence when excited under either the ultraviolet light or the cathode rays. So far less information is available concerning the Ln^{3+}-doped $CaIn_2O_4$ phosphors, and the luminescence mechanisms have not been well characterized [19,20].

The Pechini sol–gel method is a useful and attractive technique for preparation of oxide-based materials especially complex metal oxide. It has many advantages, such as homogeneous mixing of the staring materials at the molecular level the gel and the low synthetic temperature, good control of stoichiometry, fine particle size and uniform morphology [21,22]. Accordingly, in the present paper, we report the synthesis of $CaIn_2O_4$:Dy^{3+}, $CaIn_2O_4$:Pr^{3+} and $CaIn_2O_4$:Tb^{3+} phosphors via a Pechini-type sol–gel process, and investigate their luminescence properties in detail. It is of interest and significance to find that there exists an efficient energy transfer from the $CaIn_2O_4$ host lattice to the doped Dy^{3+}, Pr^{3+} and Tb^{3+} ions, resulting in strong bluish white (Dy^{3+}), and green (Pr^{3+} and Tb^{3+}) emission, respectively. These phosphors are potentially applied for FEDs.

2. Experimental

The undoped $CaIn_2O_4$, $CaIn_2O_4$:Dy^{3+}, $CaIn_2O_4$:Pr^{3+} and $CaIn_2O_4$:Tb^{3+} samples were prepared by a Pechini-type sol–gel process [14,23]. The doping concentrations of Dy^{3+}, Pr^{3+} and Tb^{3+} are 0.01–2 at% of In^{3+} in $CaIn_2O_4$. The stoichiometric amounts of $CaCO_3$ (A. R. Beijing Fine Chemical Company, China), Dy_2O_3, Tb_4O_7, and Pr_6O_{11} (99.99%, all these oxides purchased from Shanghai Yuelong Non-Ferrous Metals Limited, China) were dissolved in dilute HNO_3 (analytical reagent, A. R. Beijing Fine Chemical Company, China) under stirring and heating, resulting in the formation of colorless solutions of $Ca(NO_3)_2$, $Dy(NO_3)_3$, $Tb(NO_3)_3$ and an apple green solution of $Pr(NO_3)_3$, respectively. The solutions of $Ca(NO_3)_2$, $Dy(NO_3)_3$ [or $Tb(NO_3)_3$, or $Pr(NO_3)_3$] were mixed together followed by the addition of the stoichiometric amounts of $In(NO_3)_3 \cdot 4.5H_2O$ (A. R. Beijing Fine Chemical Company, China) under stirring. Then citric acid and polyethylene glycol (PEG, molecular weight = 10,000) were dissolved in the above solution ($C_{PEG} = 0.01$ M, citric acid/metal ion = 2:1). The resultant mixtures were stirred for 1 h and condensed at 75 °C in a water bath until dry gels formed. After being dried in oven at 110 °C for 10 h, the gels were ground and prefired at 450 °C for 4 h in air. Then the samples were fully ground and fired to the desired temperatures (700–1000 °C) for 3 h.

The X-ray diffraction (XRD) measurements were carried out on a Rigaku-Dmax 2500 diffractometer using Cu$K\alpha$ radiation ($\lambda = 0.15405$ nm). The morphologies of the samples were inspected by a field emission scanning electron microscope (FE-SEM, XL30, Philips). Diffuse reflectance spectra were taken on a Hitachi U-4100 spectrophotometer. The PL excitation and emission spectra were measured on a Hitachi F-4500 spectrophotometer equipped with a 150 W Xenon lamp as the excitation source. The cathodoluminescent (CL) measurements were carried out in an ultra-high-vacuum chamber ($<10^{-8}$ Torr), where the phosphors were excited by an electron beam at a voltage range of 1–5 kV with different filament currents (14–18 mA), and the spectra were recorded on an F-4500 spectrophotometer. The luminescence decay curves were obtained from a Lecroy Wave Runner 6100 Digital Osilloscope (1 GHz) using a tunable laser (pulse width = 4 ns, gate = 50 ns) as the excitation (Continuum Sunlite OPO). The electrical conductivity measurements were performed by dc four-probe technique in air. The powder samples were pressed into rectangular (2 mm × 5 mm × 25 mm) under a pressure of 175 MPa, and then fired at 1573 K for 8 h for conductivity measurements. Pellets have relative densities of 80–85% of the theoretical value. All the measurements were performed at room temperature (RT).

3. Results and discussion

3.1. Crystallization behavior and morphology

The crystallization behavior and morphology of the studied samples were performed representatively on

$CaIn_2O_4$:Dy^{3+} by XRD and FE-SEM, respectively. The results for $CaIn_2O_4$, $CaIn_2O_4$:Pr^{3+} and $CaIn_2O_4$:Tb^{3+} are similar to those of $CaIn_2O_4$:Dy^{3+}.

3.1.1. XRD

The XRD patterns of the $CaIn_2O_4$:0.015Dy^{3+} sample annealed at various temperatures are shown in Fig. 1. For the sample annealed at 700 °C (a), only In_2O_3 and CaO phases are present, and no diffraction peak of $CaIn_2O_4$ can be seen. The diffraction peaks of $CaIn_2O_4$ appeared after being annealed at 800 °C (b), indicating that $CaIn_2O_4$ began to crystallize at this temperature. Single phase of $CaIn_2O_4$ with orthorhombic structure was obtained after being annealed at 900–1000 °C (c–d). This observation is consistent with what reported by Dali et al. [18]. All the diffraction peaks of the $CaIn_2O_4$:0.015Dy^{3+} samples annealed at 900 °C (or higher temperature) agree well with the standard data of $CaIn_2O_4$ (JCPDS 17-0643). The crystallinity of $CaIn_2O_4$ phase increased with the increase of annealing temperatures, as confirmed by the change in full-width at the half-maximum (FWHM). No second phase was detected at the current doping level, indicating that the Dy^{3+} can be completely dissolved in the $CaIn_2O_4$ host lattice. Comparing with the conventional solid-state reaction (1400 °C for 24 h), the crystallization temperature is low [19,20]. The $Ca(NO_3)_2$ and $In(NO_3)_3$ are homogeneously mixed at the molecular level and homogeneously dispersed in the PEG precursor gel that promotes the formation of $CaIn_2O_4$ at relatively low annealing temperature.

The crystallite size of the samples can be estimated from the Scherrer equation, $D = 0.941\lambda/\beta\cos\theta$, where D is the average grain size, λ is the X-ray wavelength (0.15405 nm), θ and β are the diffraction angle and FWHM of an observed peak, respectively [24]. The strongest peak (121) at $2\theta = 33.32^\circ$ was used to calculate for the average crystallite size (D) of the $CaIn_2O_4$:0.015Dy^{3+} particles annealed at 1000 °C. The estimated average crystallite size is about 59 nm.

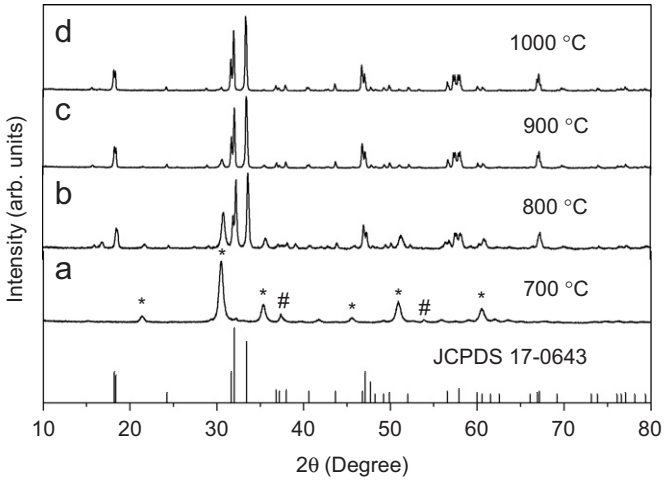

Fig. 1. XRD patterns of $CaIn_2O_4$:0.015Dy^{3+} sample annealed at different temperatures. The standard data for $CaIn_2O_4$ (JCPDS No. 17-0643) was used as reference (*In_2O_3, #CaO).

3.1.2. FE-SEM

Fig. 2 shows the FE-SEM micrograph of the $CaIn_2O_4$:0.015Dy^{3+} sample annealed at 1000 °C. It is seen clearly that the $CaIn_2O_4$:0.015Dy^{3+} samples are composed of aggregated particles with size ranging from 200 to 400 nm and approximate spherical morphology. The crystallite size estimated from XRD is 59 nm, which indicating that the $CaIn_2O_4$:0.015Dy^{3+} samples are polycrystallines consisting of several single crystallite units.

3.2. Photoluminescence properties

Fig. 3 shows the excitation and emission spectra of the $CaIn_2O_4$:0.015Dy^{3+} sample annealed at 1000 °C. The excitation spectrum of the $CaIn_2O_4$:0.015Dy^{3+} sample (Fig. 3a) monitored with 493 nm emissions of Dy^{3+} ($^4F_{9/2}$–$^6H_{15/2}$) consists of a strong excitation band from 200 to 325 nm with a maximum at 288 nm and some weak lines (356, 370, 391, 430, 455 nm) in the longer wavelength region. Clearly, the latter is due to the f–f transitions (356 nm: $^6H_{15/2}$–$^6P_{7/2}$; 370 nm: $^6H_{15/2}$–$^6P_{5/2}$; 391 nm: $^6H_{15/2}$–$^6M_{21/2}$; 430 nm: $^6H_{15/2}$–$^6G_{11/2}$; 455 nm: $^6H_{15/2}$–$^6I_{15/2}$) of Dy^{3+} within its $4f^9$ configuration [13,14]. Under 288 nm UV excitation, the $CaIn_2O_4$:0.015Dy^{3+} sample shows a strong blue–white luminescence. The emission spectrum (Fig. 3b) of $CaIn_2O_4$:0.015Dy^{3+} consists of a weak blue emission band and the characteristic emission lines of Dy^{3+}. In order to identify the origin of the weak blue emission band of the $CaIn_2O_4$:0.015Dy^{3+} phosphor, we measured the emission spectrum of the undoped $CaIn_2O_4$ sample under the same excitation condition (288 nm). It shows a weak blue emission ranging from 300 to 650 nm with a maximum at 450 nm (Fig. 3b red line). The weak blue emission of $CaIn_2O_4$ can be attributed to the recombination of an electron on a donor formed by

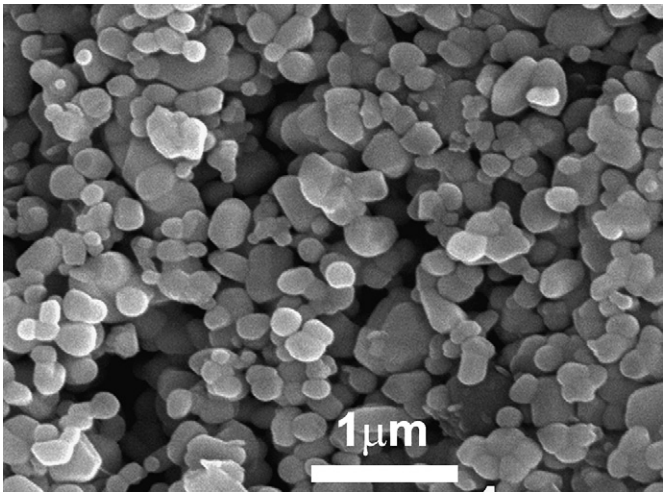

Fig. 2. FE-SEM micrograph of the $CaIn_2O_4$:0.015Dy^{3+} sample annealed at 1000 °C.

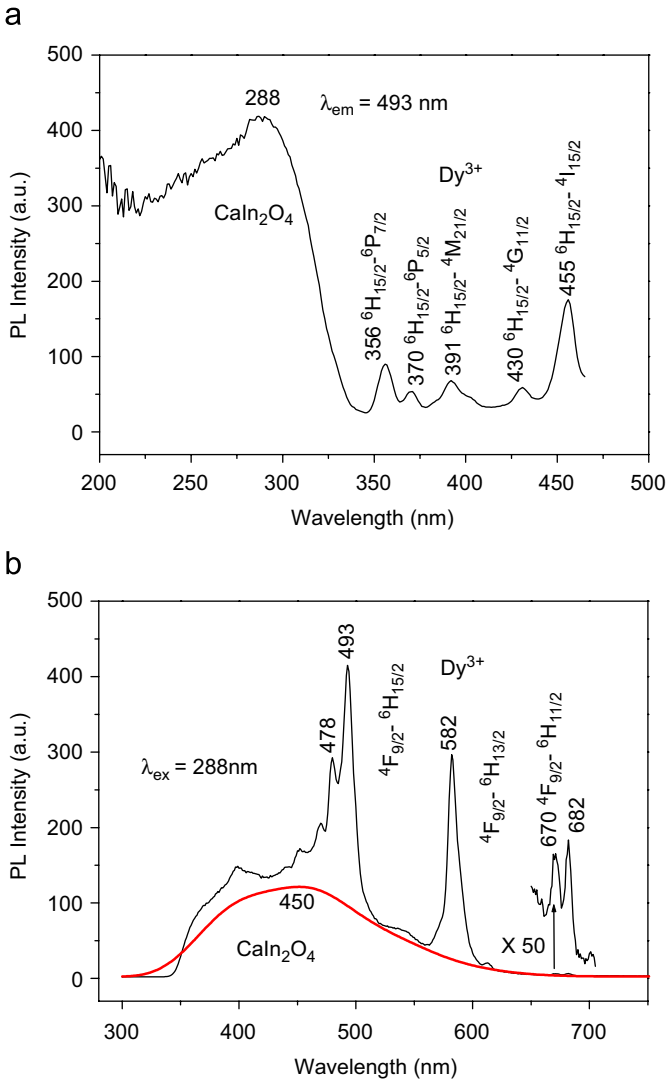

Fig. 3. Excitation (a) and emission (b) spectra of the $CaIn_2O_4$:0.015Dy^{3+}, as well as the emission spectrum of the $CaIn_2O_4$ (red line) annealed at 1000 °C.

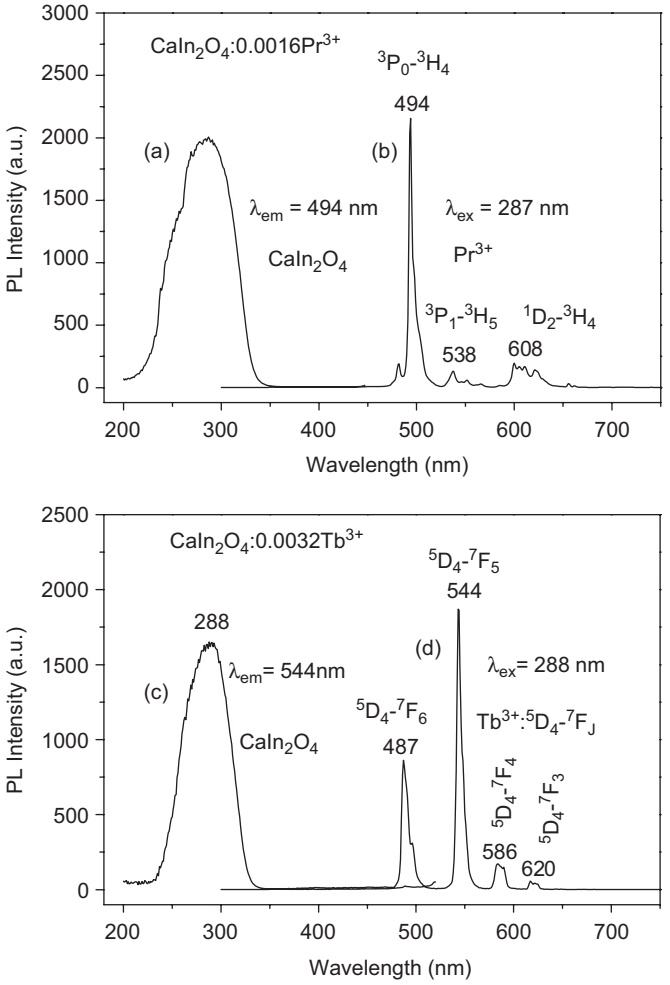

Fig. 4. Excitation and emission spectra of the $CaIn_2O_4$:0.0016Pr^{3+} (a, b) and the $CaIn_2O_4$:0.0032Tb^{3+} (c, d) phosphors.

oxygen vacancies with a hole on an acceptor consisting of either strontium vacancies or indium vacancies [25]. The weak blue emission band in $CaIn_2O_4$:0.015Dy^{3+} phosphor has the identical profile with that of the undoped $CaIn_2O_4$ (shown in Fig. 3b red line for comparison); thus, it can be ascribed to the host emission. The emission spectrum of Dy^{3+} is dominated by two main groups of emission in the blue (460–505 nm) and yellow (570–600 nm) region accompanied by a group of weak lines in the red region from 650 to 700 nm (can be seen by 50 times magnification). These emissions correspond to the transitions from $^4F_{9/2}$ to $^6H_{15/2}$, $^6H_{13/2}$ and $^6H_{11/2}$ of Dy^{3+}, respectively [13,14]. The crystal-splitting components of Dy^{3+} emission can be observed, but not totally resolved due to the weak experimental resolution.

Fig. 4 shows the excitation and emission spectra of the $CaIn_2O_4$:0.0016Pr^{3+} (a, b) and $CaIn_2O_4$:0.0032Tb^{3+} (c, d) annealed at 1000 °C, respectively. Under the excitation of short ultraviolet, the $CaIn_2O_4$:0.0016Pr^{3+} exhibits a strong green luminescence. The excitation spectrum of the as-prepared $CaIn_2O_4$:0.0016Pr^{3+} phosphor (Fig. 4a) monitored with 494 nm emission of Pr^{3+} ($^3P_0$–$^3H_4$) shows a strong excitation band with maximum at 287 nm. The emission spectrum (Fig. 4b) exhibits typically narrow lines containing three major groups in the blue, green and the red spectral regions, respectively. The emission lines peaking at 494, 538 and 608 nm are assigned to the *f–f* transitions of Pr^{3+} from $^3P_0$ to $^3H_4$, $^3P_1$ to $^3H_5$ and from $^1D_2$ to $^3H_4$, respectively, with $^3P_0$–$^3H_4$ (494 nm) as the most prominent group [19]. Tb^{3+}-doped $CaIn_2O_4$ phosphors also show a strong green emission upon the excitation into 288 nm. Similar to those of $CaIn_2O_4$:0.015Dy^{3+} and $CaIn_2O_4$:0.0016Pr^{3+}, the excitation spectrum of $CaIn_2O_4$:0.0032Tb^{3+} (Fig. 4c) monitored with 544 nm emission of Tb^{3+} ($^5D_4$–$^7F_5$) shows a strong excitation band with maximum at 288 nm. The corresponding emission spectrum (Fig. 4d) of $CaIn_2O_4$:0.0032Tb^{3+} consists of *f–f* transition lines of Tb^{3+} within its $4f^8$ electron configuration, i.e., $^5D_4$–$^7F_6$ (487 nm) in the blue region and $^5D_4$–$^7F_5$

(544 nm, strongest one) in the green region, as well as $^5D_4$–$^7F_4$ (586 nm), $^5D_4$–$^7F_3$ (620 nm) in the red region [26].

There are three possibilities for the excitation bands of the $CaIn_2O_4$:0.015Dy^{3+}, $CaIn_2O_4$:0.0016Pr^{3+} and $CaIn_2O_4$:0.0032Tb^{3+} phosphors: the host lattice absorption, the charge-transfer transition and the $4f^n \rightarrow 4f^{n-1}5d$ transitions of the rare earth ions in the Dy^{3+}/Pr^{3+}/Tb^{3+}-doped $CaIn_2O_4$ phosphors. To identify which types they belong to, we measure the diffuse reflectance spectra of the as prepared $CaIn_2O_4$, $CaIn_2O_4$:0.015Dy^{3+}, $CaIn_2O_4$:0.0016Pr^{3+} and $CaIn_2O_4$:0.0032Tb^{3+} samples, respectively, as shown in Fig. 5a–d. The four diffuse reflectance spectra have the identical profile. The strong absorption bands around 285 nm are due to the electron transition from valence bands (VB) (consisting of the 2*p* orbital of O) to the conduction bands (CBs) (consisting of the 5*s* and 5*p* orbital of In) [27], which are in agreement with the excitation spectra of the $CaIn_2O_4$:0.015Dy^{3+} (Fig. 3a), $CaIn_2O_4$:0.0016Pr^{3+} (Fig. 4a) and $CaIn_2O_4$:0.0032Tb^{3+} (Fig. 4c) samples. This indicates that all the strong excitation bands (287–288 nm) of the $CaIn_2O_4$:0.015Dy^{3+}, $CaIn_2O_4$:0.0016Pr^{3+} and $CaIn_2O_4$:0.0032Tb^{3+} arise from the host lattice absorption. The presence of the $CaIn_2O_4$ host band in the excitation spectra of Dy^{3+}, Pr^{3+} and Tb^{3+} doped $CaIn_2O_4$ phosphors indicates that an energy transfer takes place from the $CaIn_2O_4$ host lattice to the doped Dy^{3+}, Pr^{3+} and Tb^{3+} ions, i.e., the rare earth emission arises from a host sensitizing effect, as reported previously in YVO_4:Dy^{3+} and β-Ga_2O_3:Dy^{3+} [14,25]. The energy transfer efficiency can be calculated according to the formula $\eta_{ET} = 1 - I_d/I_{d0}$, where I_d and I_{d0} are the corresponding luminescence intensities of the donor (host lattice $CaIn_2O_4$) in the presence and absence of the acceptor (doping rare earth ions, Dy^{3+}, Pr^{3+} and Tb^{3+}), respectively [28]. The energy transfer efficiency of the $CaIn_2O_4$:0.015Dy^{3+} is around 76%, while those for $CaIn_2O_4$:0.0016Pr^{3+} and $CaIn_2O_4$:0.0032Tb^{3+} are close to 100% (neglect the quenching by other unknown factors).

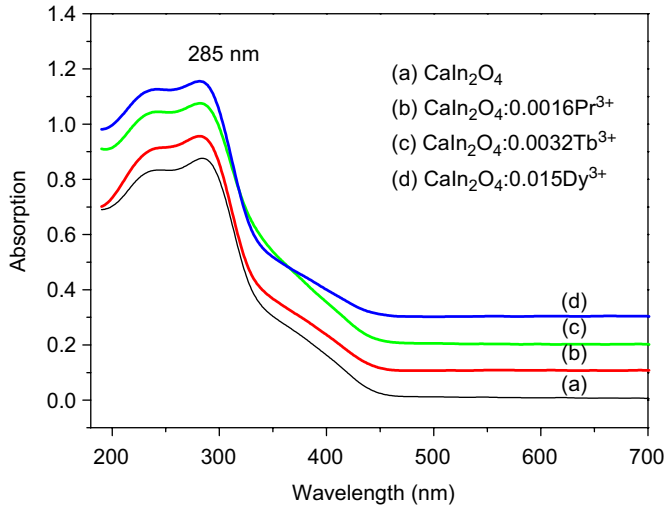

Fig. 5. Diffuse reflectance spectra of $CaIn_2O_4$ (a), $CaIn_2O_4$:0.0016Pr^{3+} (b), $CaIn_2O_4$:0.0032Tb^{3+} (c) and $CaIn_2O_4$:0.015Dy^{3+} (d) samples annealed at 1000 °C.

A simple model illustrating the blue emission process in $CaIn_2O_4$ and the energy transfer to Dy^{3+}, Pr^{3+} and Tb^{3+} is shown in Fig. 6. Under the excitation of a 288 nm (or 287 nm) irradiation (bandgap excitation), an electron (●) is excited from the VB to the CB. The electron (●) moves freely around the CB, finally relaxes to the donor band (oxygen vacancies). The recombination of the electron in the donor band with the acceptor (calcium vacancies or indium vacancies) yields a blue emission with a maximum wavelength at 450 nm (Fig. 6, left). When Dy^{3+} (Pr^{3+} or Tb^{3+}) is present in $CaIn_2O_4$ host lattices, the excitation energy can be nonradiatively transferred to Dy^{3+} (Pr^{3+} or Tb^{3+}), resulting in the characteristic emission of Dy^{3+} (Pr^{3+} or Tb^{3+}), as shown in Fig. 6 (right). The blue emission of $CaIn_2O_4$ host lattices has been quenched when a low concentration of Pr^{3+} (0.08 at% of In^{3+}) or Tb^{3+} (0.16 at% of In^{3+}) was introduced, indicating that the

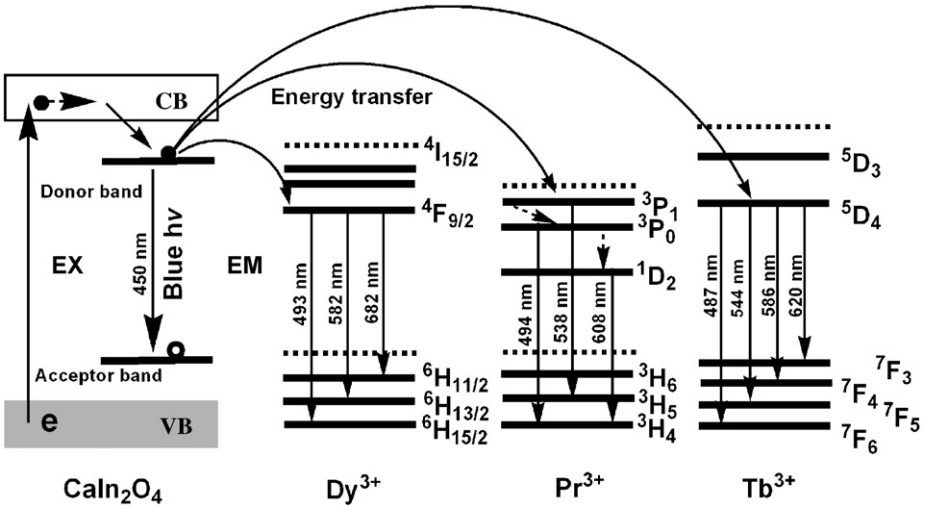

Fig. 6. A simple model illustrating the blue emission process in $CaIn_2O_4$ and the energy transfer process from $CaIn_2O_4$ to Dy^{3+}, Pr^{3+} and Tb^{3+}.

energy transfer from $CaIn_2O_4$ to Pr^{3+} and Tb^{3+} is very efficient and complete. However for $CaIn_2O_4$: $0.015Dy^{3+}$, the weak blue emission from $CaIn_2O_4$ host lattice can still be observed in the emission spectrum (Fig. 3b), suggesting that the energy transfer from $CaIn_2O_4$ to Dy^{3+} is not complete.

Fig. 7a–d shows the luminescence decay curves of the $CaIn_2O_4$, $CaIn_2O_4$:$0.015Dy^{3+}$, $CaIn_2O_4$:$0.0016Pr^{3+}$ and $CaIn_2O_4$:$0.0032Tb^{3+}$ annealed at 1000 °C, respectively. For the undoped $CaIn_2O_4$, the emission (450 nm) decays very fast. The decay curve can be fitted to a single exponential function as $I = I_0 \exp(-t/\tau)$, in which τ is the decay lifetime. The lifetime was determined to be 5.7 ns (Fig. 7a), a characteristic value for the luminescence of exciton [25]. The luminescence decay curves of Dy^{3+} ($^4F_{9/2}$–$^6H_{15/2}$), Pr^{3+} ($^3P_0$–$^3H_4$) and Tb^{3+} ($^5D_4$–$^7F_5$) in $CaIn_2O_4$ (shown in Fig. 7b–d, respectively) can also be fitted to a single exponential function. The lifetimes of Dy^{3+} ($^4F_{9/2}$ level), Pr^{3+} ($^3P_0$ level) and Tb^{3+} ($^5D_4$ level) in $CaIn_2O_4$ host were determined to be 0.75 ms, 106.80 μs and 1.51 ms, respectively, which are in the same order of magnitude as reported previously [19,25,29]. Generally speaking, if there is one kind of luminescence center in the phosphor, the decay function can be fit by the first order. Two kinds of luminescence centers means second order and so on. Furthermore, the decay behavior can also be influenced by the energy transfer and impurities present in the host lattices. The decay curves in Fig. 7a–d can fitted with an exponential decay function of first

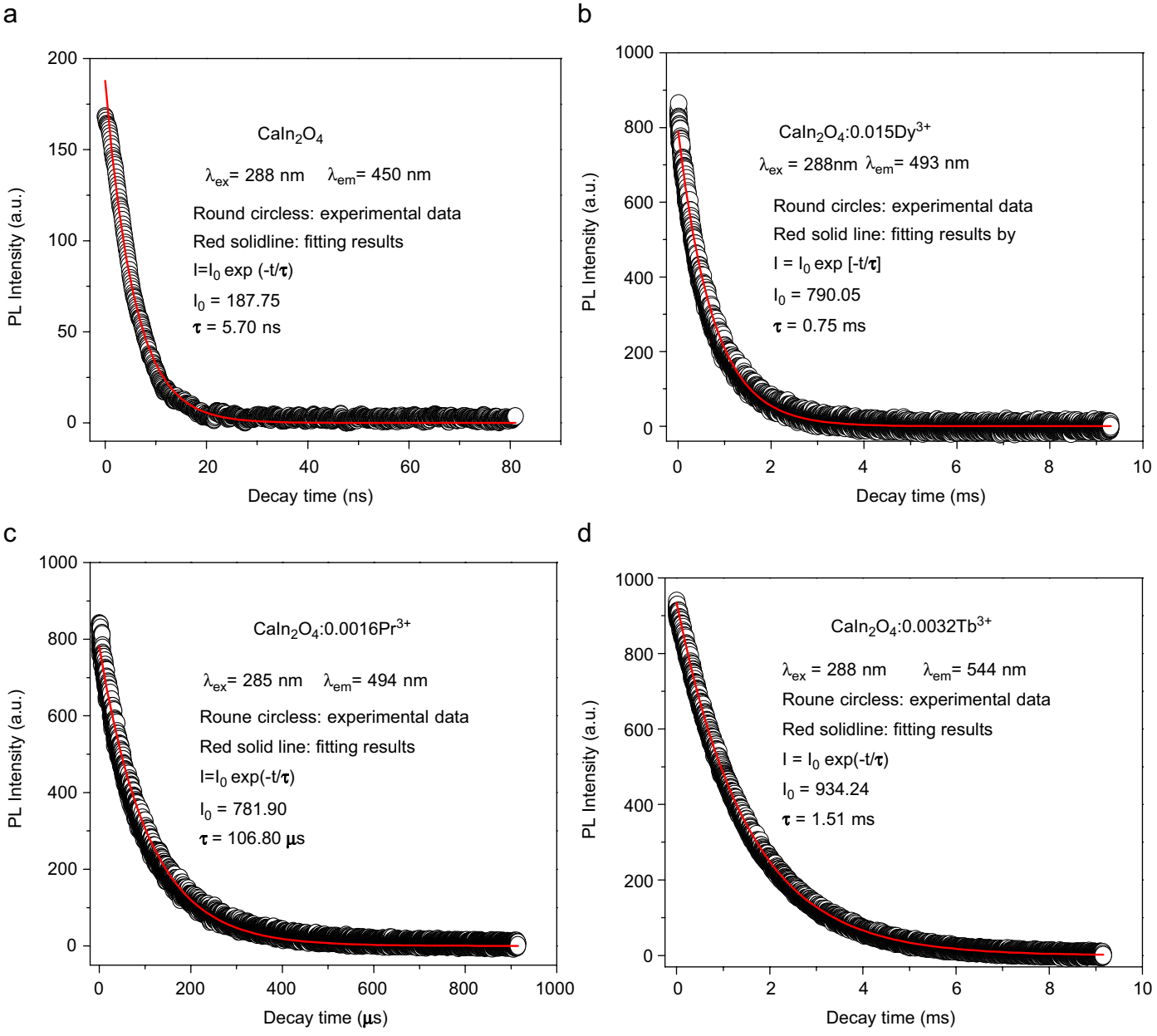

Fig. 7. The luminescence decay curves for $CaIn_2O_4$ (a), $CaIn_2O_4$:$0.015Dy^{3+}$ (b), $CaIn_2O_4$:$0.0016Pr^{3+}$ (c) and $CaIn_2O_4$:$0.0032Tb^{3+}$ (d) samples annealed at 1000 °C.

order, which is due to the homogenous environment of the activator ions (i.e., only one kind of emission center presents in the host lattice). The Commission International d'Eclairage (CIE) chromaticity coordinates of the as prepared $CaIn_2O_4$:0.015Dy^{3+} samples are $x = 0.2264$ and $y = 0.2495$ in the blue–white emission zone. For $CaIn_2O_4$:0.0016Pr^{3+} and $CaIn_2O_4$:0.0032Tb^{3+} sample, the CIE chromaticity coordinates are $x = 0.2688$, $y = 0.4193$ for Pr^{3+} and $x = 0.2569$, $y = 0.5664$ for Tb^{3+} (in the green emission zone).

The PL intensity and lifetimes of Dy^{3+}, Pr^{3+} and Tb^{3+} have been studied as a function of their doping concentration (x) in $CaIn_{2(1-x)}O_4$:2$x$$Dy^{3+}$, $CaIn_{2(1-x)}O_4$:2$x$$Pr^{3+}$ and $CaIn_{2(1-x)}O_4$:2$x$$Tb^{3+}$ samples, respectively, as shown in Fig. 8. The PL emission intensity and lifetimes of Dy^{3+} increased with the increase of its concentration (x) first, reaching a maximum value at $x = 7.5 \times 10^{-3}$, and then decreased with increasing its concentration (x) due to the concentration quenching effect (shown in Fig. 8a). Thus, the optimum concentration for Dy^{3+} is 7.5×10^{-3} of In^{3+} in the $CaIn_2O_4$ host. In general, the concentration quenching of luminescence is due to the energy migration among the activator ions at the high concentrations. In the energy migration process the excitation energy will be lost at a killer or quenching site, resulting in the decrease of PL intensity and lifetime [13]. The concentration quenching of Dy^{3+} luminescence is mainly caused by cross relaxation, i.e., energy transfers from one Dy^{3+} to another neighbor Dy^{3+} by transition that matched in energy. These transitions are mainly $Dy^{3+}(^4F_{9/2}) + Dy^{3+}(^6H_{15/2}) \rightarrow Dy^{3+}(^6F_{3/2}) + Dy^{3+}(^6F_{11/2})$ [14]. The same situation holds for the $CaIn_2O_4$:Pr^{3+} and $CaIn_2O_4$:Tb^{3+} phosphors. The optimum concentrations for Pr^{3+} and Tb^{3+} are 8.0×10^{-4} and 1.6×10^{-3} of In^{3+} in the $CaIn_2O_4$ host, respectively (shown in Fig. 8b,c). The $^3P_0$ and the $^1D_2$ emission of Pr^{3+} can be quenched by the following cross-relaxations, i.e., $Pr^{3+}(^3P_0) + Pr^{3+}(^3H_4) \rightarrow Pr^{3+}(^1D_2) + Pr^{3+}(^3H_6)$, and $Pr^{3+}(^1D_2) + Pr^{3+}(^3H_4) \rightarrow Pr^{3+}(^1G_4) + Pr^{3+}(^3F_4)$, respectively. Like the $CsCdBr_3$:Tb^{3+} and the $LnBO_3$:Tb^{3+} phosphors, the spectral energy distribution of Tb^{3+} emission is concentration independent in $CaIn_2O_4$:Tb^{3+} phosphors, i.e., at low concentration $^5D_3$–^7F_J dominates while at high concentration $^5D_4$–^7F_J dominates [26]. The absence of blue emission ($^5D_3$–^7F_J) in $CaIn_2O_4$ might be explained by the energy level match. In Tb^{3+} energy level, the $^5D_3$ excited state is 5500 cm^{-1} higher than the $^5D_4$ excited state [13]. The emission band of the $CaIn_2O_4$ maximizes at 450 nm. The $^5D_3$–^7F_J ($J = 4, 5, 6$) transition of Tb^{3+} are located at 440, 418, 376 nm (strongest one) in Tb^{3+} doped phosphors, respectively [13,26]. The $^5D_4$–^7F_J ($J = 3, 4, 5, 6$) transitions of Tb^{3+} are located at 620, 586, 544 and 487 nm, respectively, with the strongest one located at 544 nm ($^5D_4$–$^7F_5$) of Tb^{3+}. This means that the donor band level of host lattice (450 nm) is lower than the $^5D_3$ level of Tb^{3+}, but slightly higher than the $^5D_4$ level of Tb^{3+} in the $CaIn_2O_4$:Tb^{3+}, as shown in Fig. 6. The excitation energy of the host will more likely transfer from the donor band to the $^5D_4$ excited state of Tb^{3+} instead of the $^5D_3$ excited state of Tb^{3+}, resulting in the green emission of $^5D_4$–^7F_J dominated in the emission spectrum of the $CaIn_2O_4$:Tb^{3+} phosphors in spite of the low Tb^{3+} concentration.

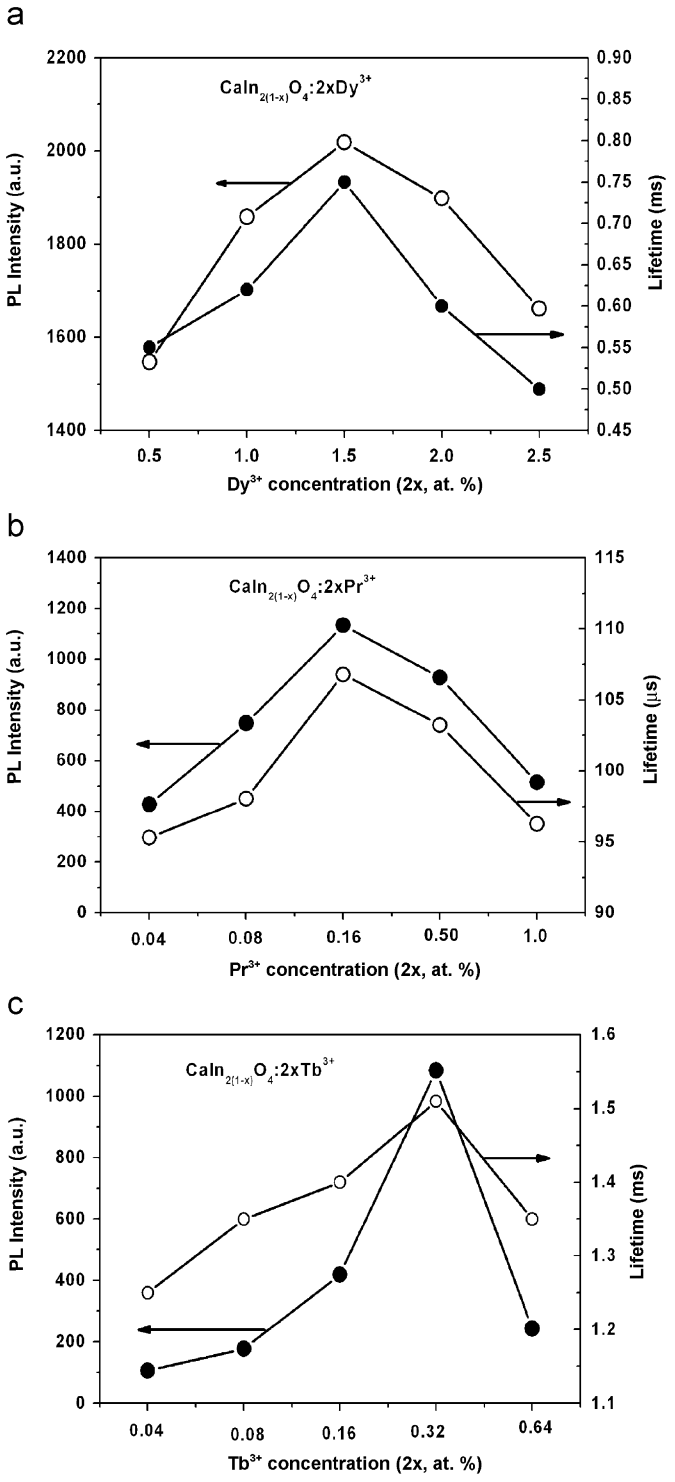

Fig. 8. The photoluminescence emission intensity and lifetimes of Dy^{3+} ($^4F_{9/2}$–$^6H_{15/2}$ and $^4F_{9/2}$–$^6H_{13/2}$), Pr^{3+} ($^3P_0$–$^3H_4$, $^1D_2$–$^3H_4$ and $^3P_1$–$^3H_5$) and Tb^{3+} ($^5D_4$–^7F_J, $J = 3, 4, 5, 6$) ions as a function of their doping concentration (x) in $CaIn_{2(1-x)}O_4$:2$x$$Dy^{3+}$, $CaIn_{2(1-x)}O_4$:2$x$$Pr^{3+}$ and $CaIn_{2(1-x)}O_4$:2$x$$Tb^{3+}$ samples, respectively (annealed temperature: 1000 °C).

Because the luminescence quenching is caused by the energy transfer among the same rare earth ions, the critical distance (R_c) can be estimated in terms of the equation, $R_c = 2(3V/4\pi NX_c)^{1/3}$ (where V is the volume of the unit cell, X_c is the critical concentration, and N is the number of available crystallographic sites occupied by the activator ions in the unit cell) [30]. The values of V and N for the crystalline $CaIn_2O_4$ ($Z = 4$, $V = abc$, $N = Z \times 2$) are 0.3500 nm^3 and 8, respectively. Considering the above optimum concentration as the critical concentration X_c, the R_c values for Dy^{3+}, Pr^{3+} and Tb^{3+} are 1.77, 3.74 and 2.97 nm in the crystalline $CaIn_2O_4$ host, respectively. Finally, it should be mentioned that optimum concentration of Dy^{3+} is much higher than those of Pr^{3+} and Tb^{3+} in $CaIn_2O_4$. The reason for this is not very clear, but most probably due to the fact that the cross relaxation effect in Dy^{3+} is not as strong as those of Pr^{3+} and Tb^{3+} in $CaIn_2O_4$.

3.3. Cathodoluminescence properties

Under low-voltage electron beam excitation, the as prepared $CaIn_2O_4$:0.015Dy^{3+} particles exhibit a white luminescence (the CIE chromaticity coordinates: $x = 0.3456$, $y = 0.3758$). Both of $CaIn_2O_4$:0.0016Pr^{3+} and $CaIn_2O_4$:0.0032Tb^{3+} samples exhibit strong green luminescence. The emission spectra for $CaIn_2O_4$:0.015Dy^{3+}, $CaIn_2O_4$:0.0016Pr^{3+} and $CaIn_2O_4$:0.0032Tb^{3+} phosphors under the excitation of electron beams are basically in line with the PL emission spectra shown in Figs. 3b, 4b and d, respectively. However, in the CL spectrum for the $CaIn_2O_4$:0.015Dy^{3+} phosphor, only the characteristic emission of Dy^{3+} is observed (the weak emission band from the host lattice is not present). For cathodoluminescence, the emission of Dy^{3+} is resulted simultaneously from the energy transfer from the $CaIn_2O_4$ host lattice and the direct excitation of Dy^{3+} by the plasmons produced by the incident electrons, while for PL the emission of Dy^{3+} is only from the former [31]. Thus, it is understandable that the Dy^{3+} emission increases, and only the characteristic emission of Dy^{3+} is observed in CL spectrum.

The CL emission intensity for the $CaIn_2O_4$:0.015Dy^{3+}, $CaIn_2O_4$:0.0016Pr^{3+} and $CaIn_2O_4$:0.0032Tb^{3+} phosphors have been investigated as a function of the accelerating voltage and the filament current, as shown in Fig. 9a and b, respectively. When the filament current is fixed at 16 mA, the CL intensity increased with raising the accelerating voltage from 1 to 5 kV (Fig. 9a). Similarly, under a 2 kV electron beam excitation, the CL intensity also increases with increasing the filament current from 14 to 18 mA (Fig. 9b). The increase in CL brightness with an increase in electron energy and filament current are ascribed to deeper penetration of electron into the phosphors body and the larger electron beam current density. The electron penetration depth can be estimated by the empirical formula: $L[\text{Å}] = 250\ (A/\rho)(E/Z^{1/2})^n$, where $n = 1.2/(1–0.29\log_{10}Z)$,

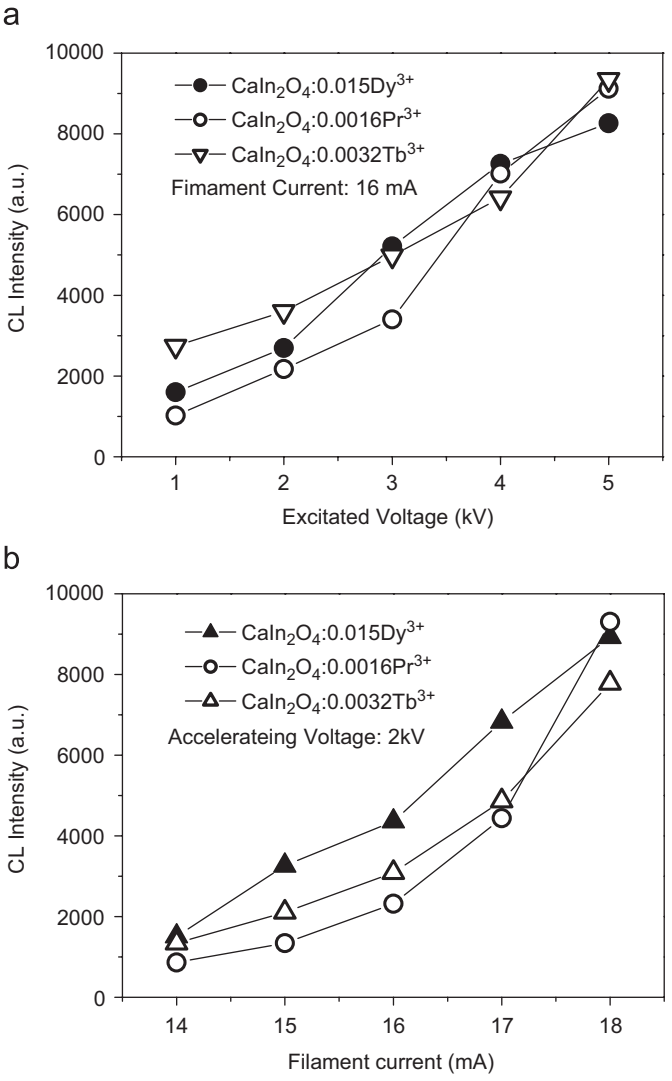

Fig. 9. The cathodoluminescence intensity of $CaIn_2O_4$:0.015Dy^{3+}, $CaIn_2O_4$:0.0016Pr^{3+} and $CaIn_2O_4$:0.0032Tb^{3+} samples as a function of accelerating voltages (a) and filament currents (b).

and A is the atomic or molecular weight of the material, ρ the bulk density, Z the atomic number or the number of electrons per molecule in the case compounds, and E the accelerating voltage (kV) [32]. For $CaIn_2O_4$:Dy^{3+}/Pr^{3+}/Tb^{3+}, $Z = 150$, $A = 333.72$, $\rho = 5.910\ g/cm^3$, the estimated electron penetration depth at 5 kV is 76.60 nm. For cathodoluminescence, the Dy^{3+}, Pr^{3+}, or Tb^{3+} ions are excited by the plasmons produced by the incident electrons. The deeper the electron penetration depth, the more the plasmons will be produced, which resulted in more Dy^{3+}, Pr^{3+} or Tb^{3+} ions being excited and thus the CL intensity increased.

The conductivities of the $CaIn_2O_4$, $CaIn_2O_4$:0.015Dy^{3+}, $CaIn_2O_4$:0.0016Pr^{3+} and $CaIn_2O_4$:0.0032Tb^{3+} samples (investigated by dc four-probe technique) were determined to be 3.0×10^{-5}, 3.8×10^{-5}, 3.5×10^{-5}, and 3.6×10^{-5} S/cm, which are much better than that of the insulator Y_2O_3 ($<10^{-12}$ S/cm). So in view of the releasing ability of

the accumulated charges on phosphors under electron beam excitation, our $CaIn_2O_4$-based phosphors should be better than Y_2O_3-based ones for the FED application. In order to test the stability of our $CaIn_2O_4$:0.015Dy^{3+}, $CaIn_2O_4$:0.0016Pr^{3+} and $CaIn_2O_4$:0.0032Tb^{3+} phosphor samples, we have measured their cathodoluminescence intensity degeneration properties under continuous electron beams excitation (for half an hour), with the Y_2O_2S:0.05Eu^{3+} phosphors as a reference. After continuous electron beams excitation for half an hour, the $CaIn_2O_4$:0.015Dy^{3+}, $CaIn_2O_4$:0.0016Pr^{3+} and $CaIn_2O_4$:0.0032Tb^{3+} still keep 88%, 92% and 90% of original intensity, but for Y_2O_2S:0.05Eu^{3+} phosphor, it only keeps 80% the of original intensity value (shown in Fig. 10a–d, respectively). The results show that our $CaIn_2O_4$-based phosphors have better stability than the Y_2O_2S based phosphors under the low-voltage excitation conditions.

4. Conclusions

The $CaIn_2O_4$, $CaIn_2O_4$:Dy^{3+} $CaIn_2O_4$:Pr^{3+} and $CaIn_2O_4$:Tb^{3+} phosphors were successfully prepared by a Pechini-type sol–gel process. Upon UV and low-voltage cathode rays excitation, the $CaIn_2O_4$:Dy^{3+} phosphors show strong blue–white/white luminescence, and the $CaIn_2O_4$:Pr^{3+} and $CaIn_2O_4$:Tb^{3+} phosphors show strong green luminescence. There exists an energy transfer from the $CaIn_2O_4$ host lattices to Dy^{3+}(Pr^{3+}, Tb^{3+}) in $CaIn_2O_4$-based phosphors,

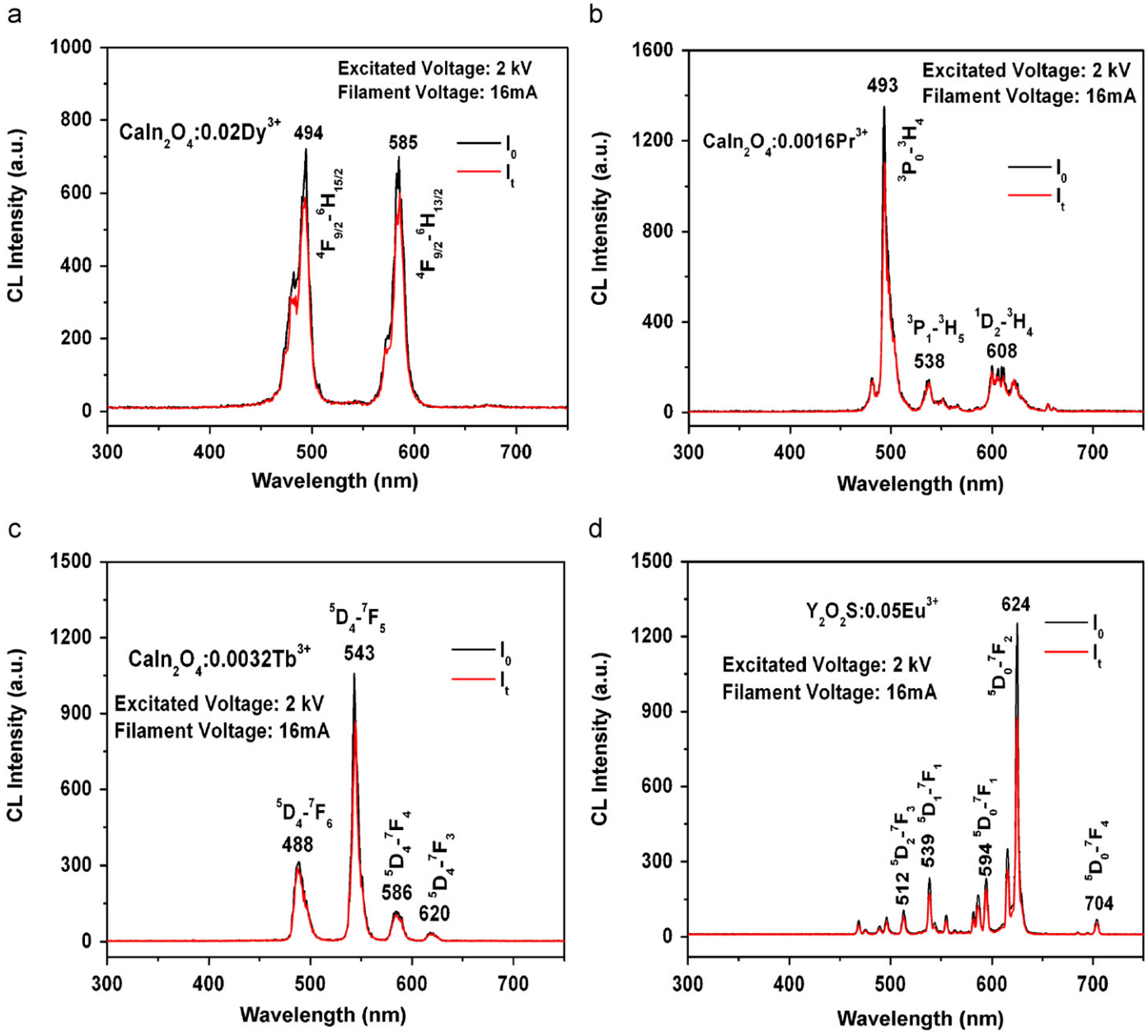

Fig. 10. Typical cathodoluminescence spectra of $CaIn_2O_4$:0.015Dy^{3+} (a) $CaIn_2O_4$:0.0016Pr^{3+} (b) $CaIn_2O_4$:0.0032Tb^{3+} (c) and Y_2O_2S:0.05Eu^{3+} (d) for comparison stability). Accelerating voltage = 2 kv (I_0: initial intensity, I_t: intensity after continuous electron beams excitation for half an hour).

respectively. The excitation energy first migrates in the host lattices and then is captured by the Dy^{3+}, Pr^{3+} or Tb^{3+}, resulting in their characteristic emissions. The optimum concentrations for the luminescence of Dy^{3+}, Pr^{3+}, Tb^{3+} are determined to be $x = 7.5 \times 10^{-3}$, 8.0×10^{-4} and 1.6×10^{-3} in $CaIn_{2(1-x)}O_4{:}2xDy^{3+}$, $CaIn_{2(1-x)}O_4{:}2xPr^{3+}$ and $CaIn_{2(1-x)}O_4{:}2xTb^{3+}$ samples, respectively. The cathodoluminescence intensity of the $CaIn_2O_4{:}Dy^{3+}$, $CaIn_2O_4{:}Pr^{3+}$ and $CaIn_2O_4{:}Tb^{3+}$ phosphors increased with raising the accelerating voltage and filament current. The higher conductivity (relative to Y_2O_3) and stability (relative to Y_2O_2S) for the $CaIn_2O_4$-based phosphors make them have potential applications in FEDs area.

Acknowledgments

This project is financially supported by the foundation of "Bairen Jihua" of Chinese Academy of Sciences, the National Natural Science Foundation of China (50225205, 50572103, 20431030) and the MOST of China (No. 2003CB314707).

References

[1] T. Jüstel, H. Nikol, C. Ronda, Angew. Chem. Int. Ed. 37 (1998) 3084.
[2] Y.D. Jing, F. Zhang, C.J. Summers, Z.L. Wang, Appl. Phys. Lett. 74 (1999) 1677.
[3] B.G. Wakefield, E. Holland, P.J. Dobson, J.L. Hutchison, Adv. Mater. 13 (20) (2001) 1557.
[4] S. Yang, C. Stoffers, F. Zhang, S.M. Jacobsen, B.K. Wagner, C.J. Summers, N. Yocom, Appl. Phys. Lett. 72 (2) (1998) 158.
[5] C.E. Hunt, A.G. Chakhovskoi, J. Vac. Sci. Technol. B 15 (2) (1997) 516.
[6] Z. Lou, J. Hao, Thin Solid Films 450 (2004) 334.
[7] P.H. Holloway, T.A. Trottier, B. Abrams, C. Kondoleon, S.L. Jones, J.S. Sebastian, W.J. Thomes, H. Swart, J. Vac. Sci. Technol. B 17 (2) (1999) 758.
[8] P. Guo, F. Zhao, G. Li, F. Liao, S. Tian, X. Jing, J. Lumin. 105 (2003) 61.
[9] A. Vecht, C. Gibbons, D. Davies, X. Jing, P. Marsh, T. Ireland, J. Silver, A. Newport, D. Barber, J. Vac. Sci. Technol. B 17 (2) (1999) 750.
[10] V.A. Bolchouchine, E.T. Goldburt, B.N. Levonovitch, V.N. Litchmanova, N.P. Sochtine, J. Lumin. 87–89 (2000) 1277.
[11] X. Jing, T. Ireland, C. Gibbons, D.J. Barber, J. Silver, A. Vecht, G. Fern, P. Trowga, D.C. Morton, J. Electrochem. Soc. 146 (12) (1999) 4654.
[12] F.L. Zhang, S. Yang, C. Stoffers, J. Penczek, P.N. Yocom, D. Zaremba, B.K. Wagner, C.J. Summers, Appl. Phys. Lett. 72 (18) (1998) 2226.
[13] G. Blasse, B.C. Grabmaier, Luminescence Materials, Springer, Berlin, Heideberg, 1994.
[14] M. Yu, J. Lin, Z. Wang, J. Fu, S. Wang, H.J. Zhang, Y.C. Han, Chem. Mater. 14 (2002) 2224.
[15] E. Loh, Phys. Rev. 147 (1966) 332.
[16] J.L. Sommerdijk, A. Bril, F.M.J.H. Hoex-Strik, Philips Res. Rep. 32 (1977) 149.
[17] J. Lin, Q. Su, J. Alloys Compds. 210 (1994) 159.
[18] S.E. Dali, V.V.S.S. Sunder, M. Jayachandra, M.J. Chockalingan, J. Mater. Sci. Lett. 17 (1998) 619.
[19] F.S. Kao, T.-M. Chen, J. Solid State Chem. 155 (2000) 441.
[20] F.S. Kao, T.-M. Chen, J. Lumin. 96 (2002) 261.
[21] M. Kakihana, J. Sol–gel Sci. Technol. 6 (1996) 7.
[22] S. Chen, X. Chen, Z. Yu, J. Hong, Z. Xue, X. You, Solid State Commun. 130 (2004) 281.
[23] M. Yu, J. Lin, J. Fu, H.J. Zhang, Y.C. Han, J. Mater. Chem. 13 (2003) 1413.
[24] Y.W. Zhang, S. Jin, S.J. Tian, G.B. Li, T. Jia, C.S. Liao, C.H. Yan, Chem. Mater. 13 (2001) 372.
[25] W.Y. Shen, M.L. Pang, J. Lin, J. Fang, J. Electrochem. Soc. 152 (2) (2005) H25.
[26] J. Lin, Q. Su, J. Mater. Chem. 5 (1995) 1151.
[27] J. Sato, H. Kobayashi, Y. Inoue, J. Phys. Chem. B 107 (2003) 7970.
[28] J.C. Bourcet, F.K. Fong, J. Chem. Phys. 60 (1974) 34.
[29] P.Y. Jia, J. Lin, X.M. Han, M. Yu, Thin Solid Films 483 (2005) 122.
[30] G. Blasse, Philips Res. Rep. 24 (1969) 131.
[31] P.Y. Jia, X.M. Liu, G.Z. Li, M. Yu, J. Fang, J. Lin, Nanotechnology 17 (2006) 734.
[32] C. Feldman, Phys. Rev. 117 (2) (1960) 455.